Journal of Sound and Vibration 389 (2017) 134–152

Contents lists available at ScienceDirect

Journal of Sound and Vibration

journal homepage: www.elsevier.com/locate/jsvi

Reconstruction and separation of vibratory field using structural holography

C. Chesnais [a,*], N. Totaro [a], J.-H. Thomas [b], J.-L. Guyader [a]

[a] Univ Lyon, INSA-Lyon, Laboratoire Vibrations Acoustique, F-69621 Villeurbanne, France
[b] Laboratoire d'Acoustique de l'Université du Maine, ENSIM, Avenue Olivier Messiaen, 72085 LE MANS Cedex9, France

ARTICLE INFO

Article history:
Received 27 June 2016
Received in revised form
17 October 2016
Accepted 24 October 2016
Handling Editor: Z Su
Available online 16 November 2016

Keywords:
Reconstruction vibratory field
Structural holography
Separation vibratory field

ABSTRACT

A method for reconstructing and separating vibratory field on a plate-like structure is presented. The method, called "Structural Holography" is derived from classical Near-field Acoustic Holography (NAH) but in the vibratory domain. In this case, the plate displacement is measured on one-dimensional lines (the holograms) and used to reconstruct the entire two-dimensional displacement field. As a consequence, remote measurements on non directly accessible zones are possible with Structural Holography. Moreover, as it is based on the decomposition of the field into forth and back waves, Structural Holography permits to separate forces in the case of multi-sources excitation. The theoretical background of the Structural Holography method is described first. Then, to illustrate the process and the possibilities of Structural Holography, the academic test case of an infinite plate excited by few point forces is presented. With the principle of vibratory field separation, the displacement fields produced by each point force separately is reconstructed. However, the displacement field is not always meaningful and some additional treatments are mandatory to localize the position of point forces for example. From the simple example of an infinite plate, a post-processing based on the reconstruction of the structural intensity field is thus proposed. Finally, Structural Holography is generalized to finite plates and applied to real experimental measurements

1. Introduction

Since decades, source localization and identification is a very important topic in both academic and industrial projects. Many methods have become an increasingly powerful research tool and allow today to understand and predict the structure behavior. However, for most of the methods, characterizing a surface requires measurements on this entire area. In this paper, a new approach in the vibratory domain is proposed to know the entire vibratory behavior of a plate with a maximum of 4 sensor lines. This method is based on the propagation and back-propagation principles, performed in the wave number domain, developed in acoustics by Williams and Maynard and called Near-field Acoustical Holography (NAH) [1].

Much research has been done to characterize and identify the vibration source acting on a structure. In the middle of 70 s, Pavic [2] and Noiseux [3] developed the structural intensimetry, defined from acoustic analogy, to analyze the flexural waves propagation in simple structures. Many publications which followed were concentrated on the structural intensity approach because the energy flow distribution gives information about the energy transmission paths, the sources positions

* Corresponding author.
E-mail address: corentin.chesnais@insa-lyon.fr (C. Chesnais).

http://dx.doi.org/10.1016/j.jsv.2016.10.042
0022-460X/

and the sinks of mechanical energy. Zhang and Mann showed that the force distribution can be calculated directly in the wavenumber domain using the two-dimensional fast Fourier transform [4], and used the measured structural intensity and the force distribution function to study vibrating plates [5]. Gavric showed the potentiality of numerical calculation of structural intensity [6] and demonstrated that this approach can be used for modal models obtained from experimental modal analysis [7,8]. Another method for localizing the excitation source is the Force Analysis Technique (FAT) introduced by Pézerat [9,10], also known as the RIFF technique, which uses a finite difference scheme to discretize the equation of motion and reconstruct the force distribution acting on structures like beams [11], plates [10] and shells [12,13]. Thereafter, FAT had also been coupled with NAH to identify vibration sources from radiated noise measurements [14]. As the Force Analysis Technique, the Virtual Fields Methods has been developed by Berry et al. [15,16] to identify and quantify the local dynamic transverse forces and distributed pressures acting on the surface of a thin plate from vibratory measurements. The main difference compared to FAT is the use of virtual fields to extract information on a part of the structure.

Initially developed for acoustic signals emitted by stationary sources [1,17,18], NAH allows now to solve more complex problems [19] and can be used for continuously visualizing nonstationary acoustic fields through RT-NAH (Real-Time Near-field Acoustic Holography) [20] or TDH (Time Domain Holography) for reconstructing sound data blocks in the time domain [21]. NAH is a powerful method to reconstruct the velocity distribution of a vibrating plate or recover the sound field of an acoustic system from the acoustic pressure hologram measured from a microphone array in the near-field. It makes it possible to visualize the spatial pressure field radiated by the system for any frequency of interest. NAH uses a specialized processing technique performed in the wavenumber domain to back-propagate the pressure field. Overcoming the ill-posed inverse problem is satisfactory done using a regularized procedure [22].

This paper presents a new reconstruction and separation vibratory field method, called Structural Holography. It is based on the back-propagation process performed in the k-space domain by using the Spatial Fourier Transform. The theory of the method leads to four coefficients identified with only four 1D sensor lines (holograms). These four coefficients allow to propagate and back propagate the wave number spectrum on the entire plate. The displacement field is obtained by applying the Inverse Spatial Fourier Transform on the wave number spectrum. If the holograms are positioned between two sources, considering the sources as forth waves or back-waves allows to separate them using Structural Holography. A source separation technique has already been applied in acoustics by Cheng et al. to separate the incident and the scattered sound fields [23]. This method is based on the principle that any waveform can be decomposed using the two-dimensional spatial Fourier transform into wave components that propagate in a known manner. The approach proposed in Structural Holography is different. The measurements are realized outside the area where the forces are localized.

In this paper, theoretical background of Structural Holography is first presented. Numerical studies and experimental results illustrate the validity of the source separation technique. A structural intensity approach is used subsequently on the reconstructed displacement to increase the accuracy of the source localization.

2. Theoretical background of structural holography

The theoretical background of Structural Holography is based on the plate bending theory. For thin plates, it is shown that the Kirchhoff theory yields accurate results. According to the Kirchhoff theory, the forced flexural vibration is governed by the following fourth-order differential equation [24]:

$$\frac{Eh^3(1+j\eta)}{12(1-\nu^2)}\left(\frac{\partial^4 w(x,y,t)}{\partial x^4}+\frac{\partial^4 w(x,y,t)}{\partial y^4}+2\frac{\partial^4 w(x,y,t)}{\partial x^2\partial y^2}\right)+\rho h\frac{\partial^2 w(x,y,t)}{\partial t^2} = F(t)\delta(x,y), \tag{1}$$

where E is the Young modulus, h the thickness of the plate, η the damping, ν the Poisson's ratio, and $w(x,y,t)$ the transverse displacement. Let us consider the example of a point force $F(t)$ located at (0,0) as expressed in Eq. (1) so that the force distribution is null anywhere else. As a consequence, Eq. (1) can be rewritten for a harmonic regime e^{jwt}:

$$\nabla^4\overline{w}(x,y)-k_f^4\overline{w}(x,y)=0, \quad (\forall\, y\neq 0) \tag{2}$$

where $\overline{w}(x,y)$ is the transverse displacement at the angular frequency ω, $k_f^4=\frac{\omega^2\rho h}{D}$ and $D=\frac{Eh^3(1+j\eta)}{12(1-\nu^2)}$. The 1D Spatial Fourier transform (SFT) is applied to Eq. (2) in x direction to obtain a 4th order differential equation:

$$\frac{\partial^4}{\partial y^4}W(k_x,y)-2k_x^2\frac{\partial^2}{\partial y^2}W(k_x,y)+(k_x^4-k_f^4)W(k_x,y)=0, \tag{3}$$

which admits the general solution:

$$W(k_x,y_i)=C^{B}_{eva}(k_x)e^{k_x^+ y_i}+C^{F}_{eva}(k_x)e^{-k_x^+ y_i} + C^{B}_{mix}(k_x)e^{k_x^- y_i}+C^{F}_{mix}(k_x)e^{-k_x^- y_i}, \tag{4}$$

where $k_x^+=\sqrt{k_x^2+k_f^2}$, $k_x^-=\sqrt{k_x^2-k_f^2}$ and y_i is the reconstruction position on the plate. This solution has four coefficients

which only depend on the wave number k_x. The coefficients C^F_{mix} and C^F_{eva} characterize forth waves, and the two others, C^B_{mix} and C^B_{eva}, represent back waves. This is the major difference with the acoustic domain where propagating waves are represented by only one coefficient as well as back propagating waves. Coefficients C^B_{eva} and C^F_{eva} characterize purely evanescent waves for all values of k_x (if k_f is real, i.e with no damping). The coefficients C^F_{mix} and C^B_{mix} define propagating waves for $k_x \leq k_f$ and evanescent waves for $k_x > k_f$. The aim of Structural Holography is to identify these four unknowns to reconstruct the whole displacement field of the plate. Thus, Structural Holography requires four 1D holograms to identify the 4 unknowns of Eq. (4). Indeed, Eq. (4) at four positions of the holograms leads to the following system of four equations:

$$\begin{pmatrix} e^{k_x^+ y_{h1}} & e^{-k_x^+ y_{h1}} & e^{k_x^- y_{h1}} & e^{-k_x^- y_{h1}} \\ e^{k_x^+ y_{h2}} & e^{-k_x^+ y_{h2}} & e^{k_x^- y_{h2}} & e^{-k_x^- y_{h2}} \\ e^{k_x^+ y_{h3}} & e^{-k_x^+ y_{h3}} & e^{k_x^- y_{h3}} & e^{-k_x^- y_{h3}} \\ e^{k_x^+ y_{h4}} & e^{-k_x^+ y_{h4}} & e^{k_x^- y_{h4}} & e^{-k_x^- y_{h4}} \end{pmatrix} \begin{pmatrix} C^B_{eva}(k_x) \\ C^F_{eva}(k_x) \\ C^B_{mix}(k_x) \\ C^F_{mix}(k_x) \end{pmatrix} = \begin{pmatrix} W(k_x, y_{h1}) \\ W(k_x, y_{h2}) \\ W(k_x, y_{h3}) \\ W(k_x, y_{h4}) \end{pmatrix}, \tag{5}$$

where $W(k_x, y_{hi})$ with $i=1.4$ is the wave number spectra on hologram i at the position y_{hi} on the y axis. Solving Eq. (5) allows us to determine the four coefficients and then to compute the wave number spectrum on the plate using Eq. (4) with varying y position values. Finally, by applying the Inverse Spatial Fourier Transform (ISFT) to the wave number spectrum, the displacement field is obtained:

$$\overline{w}(x, y) = ISFT[W(k_x, y)] = \int W(k_x, y) e^{-jk_x x} \frac{dk_x}{2\pi}. \tag{6}$$

To summarize, four steps must be followed to reconstruct the displacement on the plate by Structural Holography and they are schematized in Fig. 1:

- Measure the displacements providing the holograms
- Apply the STF to the holograms to identify the coefficients (Eq. (5))
- Compute the wave number spectrum $W(k_x, y)$ on the plate from Eq. (4)
- Apply the ISTF to the wave number spectrum to reconstruct the displacement $\overline{w}(x, y)$

One has to pay attention to the fact that the solution given by Eq. (2) is only valid in zones where no external force is applied. As a consequence, the back-propagation is conceptually limited by the position of the force.

3. Vibratory field separation principle

Let us consider now the case where two correlated point forces are acting simultaneously on the plate as presented in Fig. 2. Between positions y_i and y_j of point forces, Eq. (4) holds. Thus, inside this area, the solution of Eq. (4) is still given by Eq. (5). To determine the coefficients C^F_{mix}, C^F_{eva}, C^B_{mix}, and C^B_{eva}, four 1D holograms are located between the two point forces, as presented in Fig. 2. Solving the system of equation Eq. (5) gives access to all kind of waves traveling between y_i and y_j. As discussed in the previous part, the Structural Holography expression can be separated in two kinds of waves: the forth waves with C^F_{mix} and C^F_{eva} coefficients, and the back waves with C^B_{mix} and C^B_{eva} coefficients. As a consequence, the response of the plate due to F_i can be isolated from the one due to force F_j. To identify the plate behavior only due to source F_i, the wave number spectrum $W_{Fi}(k_x,y)$ is computed on the plate with the coefficients C^F_{mix} and C^F_{eva} only (Eq. (7)). Conversely, the response of the infinite plate only due to force F_j can be deduced using only coefficients C^B_{mix} and C^B_{eva} (Eq. (8)).

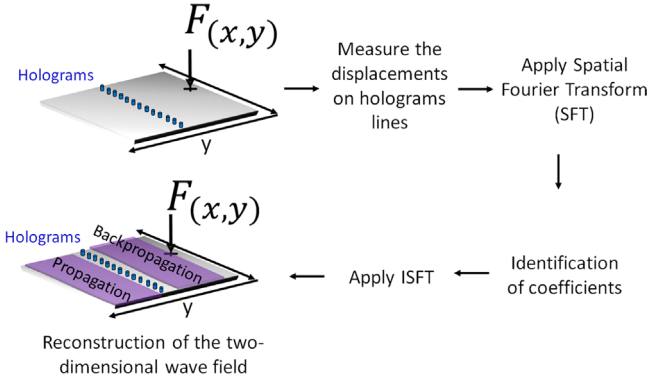

Fig. 1. Synopsys of structural holography.

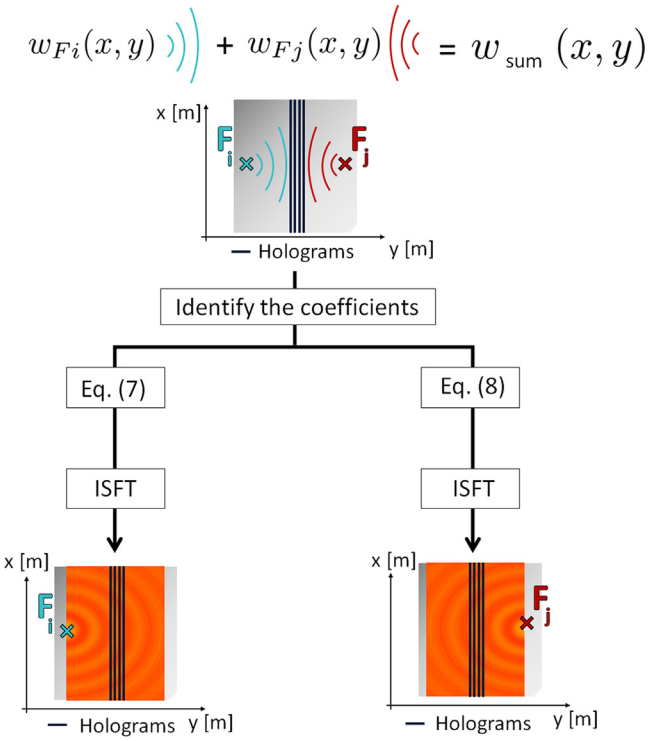

Fig. 2. Synopsys of source separation by structural holography.

$$W_{F_i}(k_x, y) = C^{F}_{eva}(k_x)e^{-k_x^{+}y} + C^{F}_{mix}(k_x)e^{-k_x^{-}y}, \tag{7}$$

$$W_{F_j}(k_x, y) = C^{B}_{eva}(k_x)e^{k_x^{+}y} + C^{B}_{mix}(k_x)e^{k_x^{-}y}. \tag{8}$$

Structural Holography is thus a vibratory field separation method for reconstructing the whole displacement field using only information measured on four lines. Some examples of this separation technique will be shown in the next sections. However, it is implicitly assumed here that the waves travelling in the plate-like structure are correlated. In case of uncorrelated sources, a cross-spectral procedure based on reference signals can be used as done by Lee et al. on aeroacoustic sources [25]. In addition, it can be underlined here that in the case of reflections on boundary conditions (finite plate), the Structural Holography only separates waves coming from the left of the holograms and those coming from the right.

4. Near-field and far-field Structural Holography

4.1. Effects of purely evanescent waves

As shown above, the theory of Structural Holography is based on four coefficients and two of them characterize purely evanescent waves whatever k_x. In the case of evanescent coefficient, the propagator is $e^{-\mathrm{Re}(k_x^{+})y}$ for the propagation process (forth waves). But it is well known that the evanescent waves quickly decrease with the distance to forces or boundary conditions [23]. As a consequence, the amplitudes of these waves can be considered as almost null at the positions of the holograms. If the estimation of these amplitudes with the holograms is disturbed by measurement noise, the back-propagation process exponentially increases the errors. Let us consider for example a forth wave composed by a propagating and an evanescent wave. If k_x=89.88 rad/m and k_f=77.84 rad/m for example, the amplitude of the evanescent wave has decreased of 99 % at a distance $d_F \simeq \lambda/2 \simeq 4$ cm from the force (Fig. 3). If the first hologram is located at only d_F=7 cm, the amplitude of the evanescent wave is less than $2{,}5.10^{-4}$ % of the initial value. Any small error in the estimation of this amplitude will be multiplied by a factor 4×10^3.

The error in the estimation of the amplitude of evanescent waves can have different origins. They can be due to:

- measurement noise,
- discretization of the hologram,
- length of the hologram (not infinite).

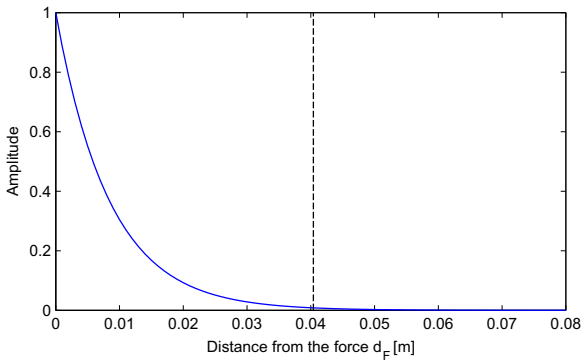

Fig. 3. Amplitude of the propagator $e^{-\mathrm{Re}(k_x^+)y}$ as a function of the distance from the force d_F. Vertical dashed lines represent $\lambda/2$.

Finally, two versions of the structural holography can be defined:

- a Near-Field Structural Holography (NSH) composed by 4 holograms. The objective of this version is to reconstruct any kind of waves including evanescent waves.
- a Far-Field Structural Holography (FSH) composed by only 2 holograms. The aim of FSH is to reconstruct only propagating field on the plate.

4.2. Far-field Structural Holography (FSH)

In the far-field, the influence of evanescent waves is neglected. Therefore they are not taken into account in FSH when holograms are positioned far from sources or boundary conditions. Consequently, only coefficients C^{B}_{mix} and C^{F}_{mix} are used to compute the wave number spectrum and Eq. (4) becomes:

$$W(k_x, y) = C^{B}_{mix}(k_x)e^{k_x^- y} + C^{F}_{mix}(k_x)e^{-k_x^- y}. \tag{9}$$

Thus, coefficients $C^{B}_{mix}(k_x)$ and $C^{F}_{mix}(k_x)$ are determined solving a linear system of two equations. This is why only two holograms are required:

$$\begin{pmatrix} e^{k_x^- y_{h1}} & e^{-k_x^- y_{h1}} \\ e^{k_x^- y_{h2}} & e^{-k_x^- y_{h2}} \end{pmatrix} \begin{pmatrix} C^{B}_{mix}(k_x) \\ C^{F}_{mix}(k_x) \end{pmatrix} = \begin{pmatrix} W_1 \\ W_2 \end{pmatrix}, \tag{10}$$

where W_i with $i=1,2$ is the wave number spectrum $W(k_x, y_{hi})$ on hologram i at position y_{hi} on y axis. Taking into account only two holograms simplifies the solution and allows to obtain the analytic formulation of the two coefficients. In the case of FSH, Eq. (9) can be expressed only as a function of distance d between holograms and distance Δ between the first hologram and the reconstruction line. Indeed, as $y_{h2} = y_{h1} + d$ and $\Delta = y - y_{h1}$, Eq. (9) becomes

$$W(k_x, y) = \left(\frac{W_2 - W_1 e^{k_x^- d}}{e^{-k_x^- d} - e^{k_x^- d}} \right) e^{k_x^- \Delta} + \left(\frac{W_1 e^{-k_x^- d} - W_2}{e^{-k_x^- d} - e^{k_x^- d}} \right) e^{-k_x^- \Delta}. \tag{11}$$

This equation only depends on d and Δ and not on the coordinates of the holograms and the reconstruction line. This equation clearly shows that it is not necessary to know the relative distance between the force and the holograms: this expression is independent of this parameter. As a consequence, FSH can be applied even if the location of forces is completely unknown.

Even if C^{F}_{eva} and C^{B}_{eva} are neglected in FSH, a part of evanescent wave behavior is still included in C^{F}_{mix} and C^{B}_{mix} when $k_x > k_f$. To cancel the influence of high wave numbers ($k_x > k_f$), a filter based on the shape of a tapered window function in k-space, called Tukey window [26], is applied on C^{F}_{mix} and C^{B}_{mix} coefficients. An example of this filter is illustrated in Fig. 4. In between $-k_f$ and $+k_f$ the wave number spectrum is not filtered (filter=1), below $-\alpha k_f$ and above $+\alpha k_f$, the spectrum is completely filtered (filter=0). In between theses zones, the spectrum is continuously decreased.

As the Fourier transforms are performed with discrete data and over a finite hologram, numerical difficulties may occur in the calculation of coefficients. Therefore, in order not to introduce disturbance during the back propagation operation, it is necessary to filter part of the evanescent waves before processing [27,28]. The previous filter, applied in the wave-number domain on the coefficients permits to overcome numerical difficulties caused by the use of the SFT [4]. The choice of a proper filter size (k_x bandwidth) is crucial [5]. If the filter size is too large, the noise may not be removed and the accessible distance for back-propagation can decrease. If the filter size is too small, useful information may be removed along with noise, and the results may not lead to the source positions [4].

To summarize, there are two major reasons to use a filter on the coefficients before computing the back-propagated wave number spectrum. A filter is necessary to decrease the effect of the propagator when k_x^- is real in the back-propagation

process (evanescent waves) and to overcome the effect due to the discretization of a finite hologram length.

An example of not filtered and filtered C^{F}_{mix} coefficient is presented in Fig. 5. This example shows the increase of the coefficient amplitude, in the high wave numbers in Fig. 5(a), and reduced by the filtering operation in Fig. 5(b).

4.3. Example of reconstruction using NSH and FSH

Examples of reconstruction using NSH and FSH on the displacement generated by one harmonic point force applied to an infinite plate are presented in this section. The application on an experimental study is presented in the last section. The transverse displacement due to one point force is given by [29]:

$$\overline{w}(x, y) = -j\frac{F}{8k_f^2 D}\left[H_0^{(1)}(k_f r) - j\frac{2}{\pi}K_0(k_f r)\right], \tag{12}$$

where $H_0^{(1)}(k_f r)$ is the Hankel function, r is the distance between the computed displacement point and the origin (0,0), $K_0(k_f r)$ is the modified Bessel function of the second kind and k_f is the wavenumber of the flexural wave in the plate. In the present example, a 1 mm thick aluminum plate ($E=69\times10^9$ Pa, $\rho=2700$ kg/m^3, $\nu=0.346$) is excited by a harmonic point force at frequency 2000 Hz. A damping of 2 % is applied and the real part of $k_f=89.88$ rad/m. Results using NSH and FSH are shown respectively in Fig. 6 when the holograms are located in the near-field of the force (distance from the point source $d_F=0.03$ m$<\lambda/2$) and in Fig. 7 when they are located in the far-field ($d_F=0.12$ m$>1.5\times\lambda$). The results are presented on y axis for x=0. The point force is located at (0,0). The reconstruction of the displacement field is clearly better with NSH when the holograms are located in the near-field of the source (Fig. 6 (a)). NSH accurately estimates the amplitude of displacement close to the force (error of 1.47% at $d_F=1$ cm) thanks to the consideration of all types of waves. However, even if the reconstruction error is 14.77 % at 1 cm from the source, the performance of FSH is surprisingly good (Fig. 6 (b)). Indeed, the estimation of the amplitude of displacement near the force is slightly underestimated due to the lack of evanescent waves in FSH but the results are still close to the reference even when the holograms are located in the near-field.

Fig. 7 presents the reconstructed displacement with the holograms positioned in the far-field. To demonstrate the disturbances due to the evanescent coefficient, the displacement reconstructed by NSH is plotted in Fig. 7(a). As explained in

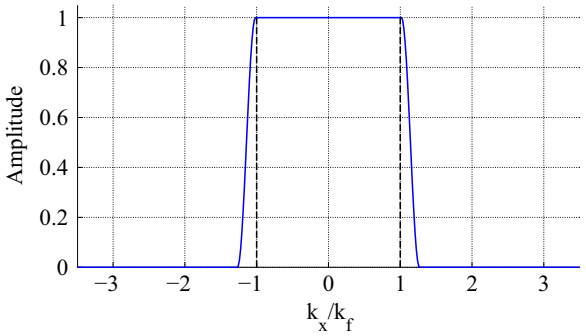

Fig. 4. Filter in non-dimensional k-space by means of k_f based on the Tukey window ($\alpha=0.25k_f$). Vertical dashed lines represent $-k_f$ and $+k_f$.

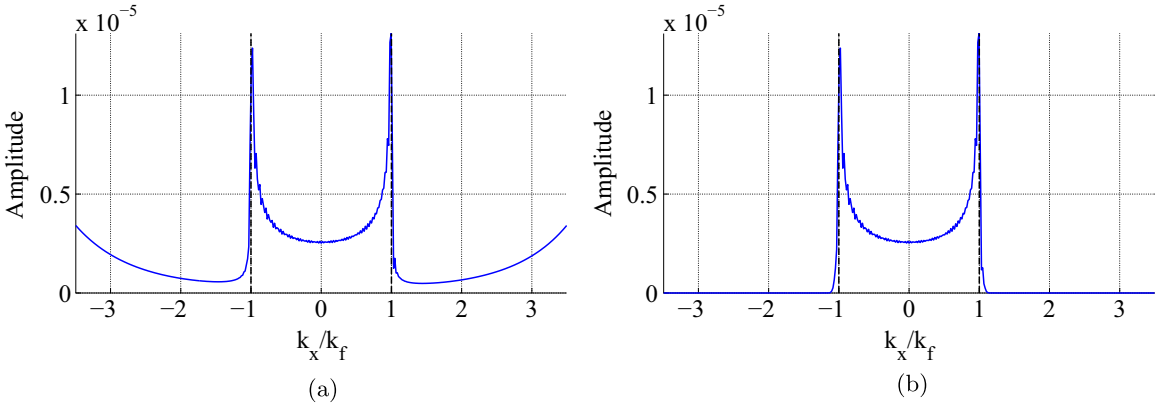

Fig. 5. Coefficient C^{F}_{mix} not filtered (a) and filtered (b) in the non-dimensional wavenumber domain by means of k_f. Vertical dashed lines represent $-k_f$ and $+k_f$.

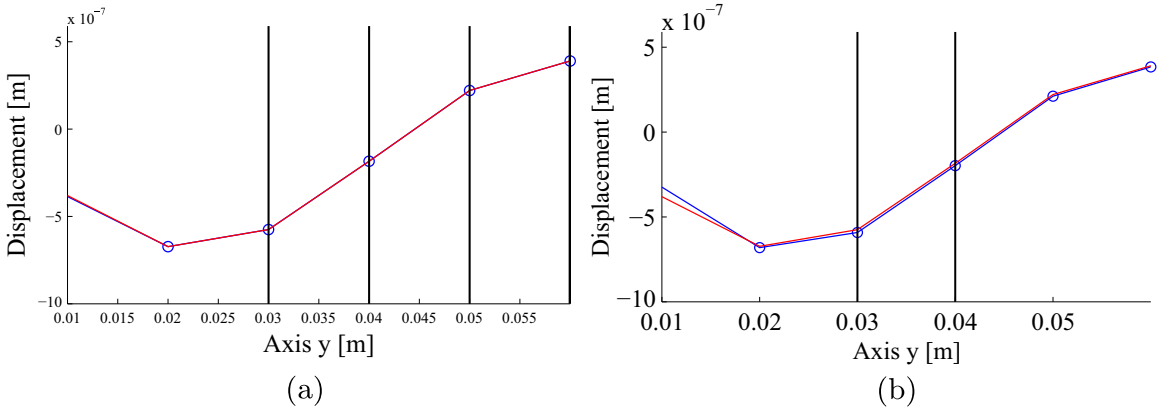

Fig. 6. Case for holograms positionned in the near-field: Reference displacement (in solid line) compared with the reconstructed forth wave (circle) (a) by NSH process and (b) by FSH process. The vertical solid lines represent the hologram positions.

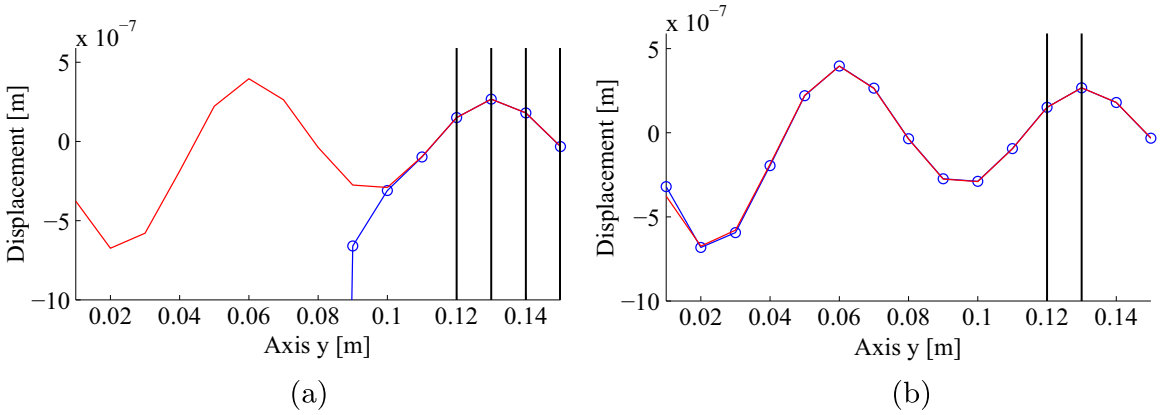

Fig. 7. Case for holograms positionned in the far-field: Reference displacement (in solid line) compared with the reconstructed forth wave (circle) (a) by NSH process and (b) by FSH process. The vertical solid lines represent the hologram positions.

Section 4.1 and illustrated in Fig. 3, evanescent waves exist only in the near-field. Taking into account the evanescent coefficient (NSH) in the far-field configuration reduces the performance of the method and does not allow to back-propagate the field up to the position of the force. The displacement is back-propagated with a low error percentage only on 2 cm, near the hologram position, but dramatically increases with the back-propagation distance (error of 139.6% at $d_F = 9$ cm in Fig. 7 (a)). The reconstructed displacement obtained with FSH is presented in Fig. 7(b) and proves the accuracy of this approach in the far-field compared to NSH. Indeed the reconstruction of the displacement field is satisfactory up to the position of the force. The reconstruction error is less than 14 % at 1 cm from the source, less than 2 % at 2 cm and less than 0.5 % beyond 7 cm. That is equivalent to the performance of FSH when the holograms are in the near-field. This demonstrates that the performance of FSH does not depend on the distance from the source.

Therefore, the use of the NSH or FSH process according to the distance to the force is an essential choice to reconstruct the displacement field with accuracy. To quantify the influence of this distance on the NSH and FSH performance, a quadratic error indicator is used. The chosen indicator is defined for a frequency band by the magnitude of the difference between the reconstructed displacement by Structural Holography (NSH and FSH) and the reference displacement, divided by the magnitude of the reference displacement:

$$Err([f_1, f_s]) = \frac{\sum_{f=f_1}^{f_s} \sum_{i}^{Ni} \sum_{j}^{Nj} \left| = \overline{w}_{holo}(x_i, y_j, f) - = \overline{w}_{ref}(x_i, y_j, f) \right|^2}{\sum_{f=f_1}^{f_s} \sum_{i}^{Ni} \sum_{j}^{Nj} \left| = \overline{w}_{ref}(x_i, y_j, f) \right|^2}, \tag{13}$$

where $[f_1, f_s]$ represents a frequency band, Ni and Nj are the number of points of the displacement along the x and y directions, $w^{rec}(x, y, f)$ is the displacement reconstructed by Structural Holography and $w_{ref}(x, y, f)$ is the reference displacement. Only the back-propagated displacement field is considered.

The quadratic error is computed on a constant domain $L_x = -0.04$ to $+0.04$ cm around the force on x dimension and on a back-propagation distance L_y only, on y dimension. As NSH is highly unstable when holograms are located in the far-field,

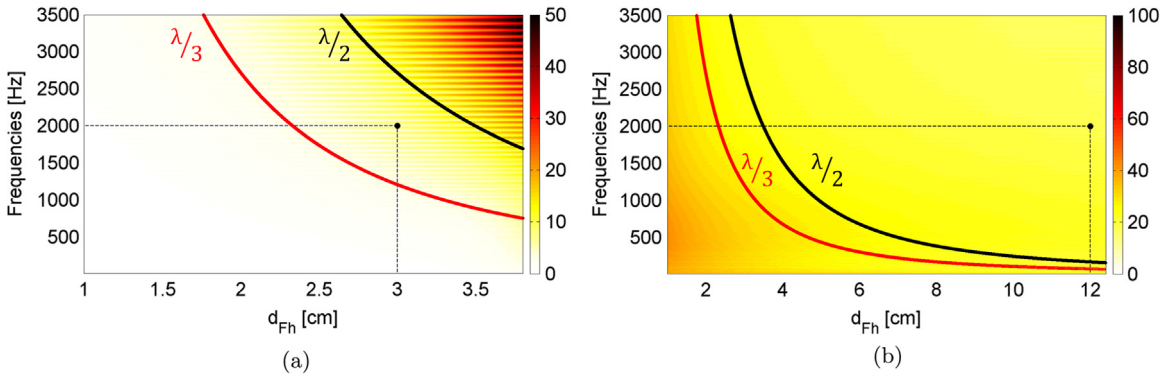

Fig. 8. Quadratic error as a function of the distance to force for the [10:3500] Hz frequency band for NSH (a) and FSH (b) formulations.

the study on d_{Fh} is limited to 1 to 4 cm. Conversely, FSH is supposed to give satisfactory results whatever the distance to the force, thus the study is done for distances from 1 to 12 cm. Results are illustrated in Fig. 8(a) for NSH and in Fig. 8(b) for FSH. The color scale indicates the error percentage. The dot in Fig. 8(a) represents the parameters which lead to the reconstructed displacement illustrated in Fig. 6(a). The dot in Fig. 8(b) represents the parameters leading to the reconstructed displacement illustrated in Fig. 7(b).

The quadratic error indicator proves that the NSH process provides in the near-field a great accuracy for the reconstruction of the displacement field. However the performance of NSH quickly declines and errors higher than 30 % are observed for distance to the force higher than $\lambda/2$. NSH process becomes inappropriate. As a consequence, NSH becomes unstable if the holograms are not located in the vicinity of the force. This conclusion implies that the position of forces should be known to apply NSH to be sure to capture evanescent waves.

Except for $d_{Fh} < \lambda/3$, FSH presents the same percentage of error whatever the frequency and the distance d_{Fh}. Applying FSH in the near-field of the force ($d_{Fh} < \lambda/3$) leads to slight error due to the presence of evanescent waves not taken into account in FSH.

To conclude, NSH is highly sensitive to the measure of the evanescent components. Beyond $\lambda/2$, the measure of these components becomes difficult and leads to huge errors in the back propagation process. However, considering the estimation of the exact amplitude of the displacement field in the vicinity of the source, NSH provides really accurate results if the holograms are in the near-field of the source. Conversely, FSH is dedicated to the reconstruction of the displacement field considering propagating waves only. FSH gives satisfactory results if the holograms are in the far-field and only slight errors if the holograms are in the near-field. In this point of view, FSH is more stable than NSH but cannot reconstruct exactly the field near the force because of the lack of evanescent waves.

4.4. *Influence of the geometric parameter*

The holograms are defined by a length L_{holo} and N points separated by Δ_x. In the acoustic domain, it is well known that NAH results are limited by these geometrical parameters due to the SFT on a finite domain [29]. These parameters define in the k-space domain:

- the wavenumber ranges from -$k_x^{\max}$ to $k_x^{\max}$, where $k_x^{\max}$ the maximum wavenumber is given by

$$k_x^{\max} = \frac{\pi}{\Delta_x}, \tag{14}$$

- the precision of the wavenumber step Δ_{kx} given by

$$\Delta_{kx} = \frac{2\pi}{L_x}. \tag{15}$$

To quantify the influence of these geometrical parameters on the NSH and FSH performance and to identify the geometrical limits, the quadratic error indicator is used (Eq. (13)). For all parametric studies, the distance between each hologram is fixed at 1 cm. For the NSH process, the hologram 1 is positioned at a distance lower than λ / 2 (y_{h1}=3 cm) to be in the near-field. For the FSH process, the hologram 1 is positionned at a distance higher than λ (y_{h1}=8 cm) to be in the far-field. The quadratic error is expressed as a percentage.

Firstly, the influence of the hologram length is evaluated. To set the size of the computed area identical whatever hologram length, the quadratic error is applied on a constant line: $L_x = -0.04$ to $+0.04$ cm around the force on x dimension and L_y is the back-propagated displacement at the distance d_{Fh}=1 cm. The hologram length L_{holo} varies from 0.4 m to 2 m.

As $\Delta_{kx} = \frac{2\pi}{L_x}$, zero padding is applied to obtain a constant wavenumber step. Therefore, only the influence of the hologram length is studied and the value Δ_{kx} = 1.57 rad/m is fixed by the zero padding process. Results are illustrated in Fig. 9(a) for NSH process and in Fig. 9(b) for FSH process.

The estimation errors in NSH and FSH are mainly observed for small holograms and high frequency. This can be explained by the wavenumber discretization step Δk_x which is too large compared to the wavenumber spectrum variations. With such small holograms, a lot of information is lost even if a zero-padding step is used.

The influence of Δ_x is also evaluated. For this study, the length of the hologram is deliberately large to avoid the influence of this physical value, therefore L_{holo}=4 m. The step Δ_x varies from 0.2 cm to 5 cm. Results are illustrated in Fig. 10(a) for NSH process and in Fig. 10(b) for FSH process. A common characteristic is visible with NSH and FSH for high frequency and large step Δ_x. As underlined by the red curves, errors quickly increase for Δ_x larger than $\frac{\lambda}{2}$. This can be set as a criterion for the spatial discretization step. The two main differences between NSH and FSH are:

- when the criterion $\Delta_x < \frac{\lambda}{2}$ is fulfilled NSH produces better estimation of displacement near the force than FSH (error almost null with NSH and near 20 % with FSH). This is essentially due to the lack of evanescent waves in FSH that underestimates displacement levels near the force.
- A zone with high error levels appears for small Δ_x with NSH. Such a zone is not present with FSH. This zone is due to the huge amplification of coefficients of NSH (Eq. (4)) in the high wave number values. The smaller Δ_x values increase the higher wave number components, taken into account into NSH resolution. The filtering step used in FSH avoid this problem.

4.5. *Influence of noise*

It is shown in Section 4.4 that the uncertainty on the estimation of the evanescent waves disturbs the back-propagation process. When noise is present during the measurement, it is more difficult to extract the useful information, which should

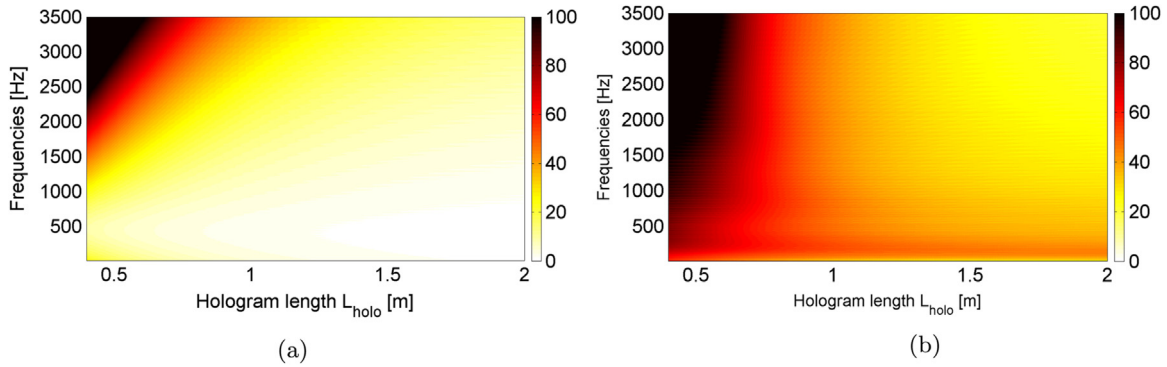

Fig. 9. Quadratic error as a function of the hologram length for the [10:3500] Hz frequency band for NSH (a) and FSH (b) formulations.

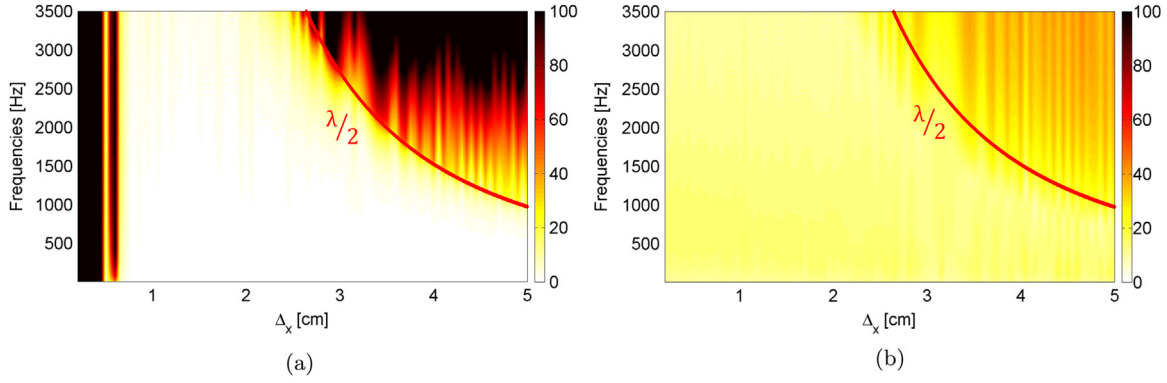

Fig. 10. Quadratic error as a function of the step Δ_x for the frequency band [10:3500] Hz for NSH (a) and FSH (b) formulations. The red line is $\lambda/2$.

decrease the performance of the method. In this section, the reconstruction error is evaluated as a function of the Signal to Noise Ratio (SNR) added to the displacements. The quadratic error is computed on a constant line: $L_x = -0.04$ to $+0.04$ cm around the force on x dimension and L_y is the back-propagated displacement at distance $d_{Fh} = 1$ cm. The study is realized at frequency f = 2000 Hz. For the NSH process, the hologram 1 is positioned at a distance shorter than $\lambda / 2$ ($y_{h1} = 3$ cm) to be in the near-field. For the FSH process, the hologram 1 is positioned at a distance higher than λ ($y_{h1} = 8$ cm) to be in the far-field. The SNR is successively set to values from 2 to 50 dB (step 0.25 dB).

Results are presented in Fig. 11 and show completely different behaviour for NSH and FSH when Signal to Noise Ratio increases. For FSH, the quadratic error is almost constant (around 25 %) whatever the SNR value. This constant error, already observed in Section 4.4, is not linked to the added noise but to the lack of evanescent waves. This error is just slightly increased for low SNR values. This demonstrates how stable is FSH according to SNR value. It is a little more than the error on the reconstruction without noise, presented in Section 4.3. Therefore, the constant error is essentially caused by not considering of the evanescent waves. Thus the method is very stable even at very high noise levels.

The NSH process is much more sensitive to measurement noise than FSH. For SNR lower than 20 dB, the quadratic error is higher than 100%. For this (not filtered) version of NSH, the experimental applicability of the method is questionable. The unstable behaviour of NSH according to the SNR value is due to the amplification of coefficients in the high wavenumber values. Filter these components (typically for $k_x > 1.75 * k_f$) should improve the stability and the applicability of NSH. However, without any filtering and as shown in Fig. 11, NSH provides better results than FSH for high SNR values. This is coherent with remarks made in Fig. 10. FSH suffers from a constant error due to the lack of evanescent waves. This is not the

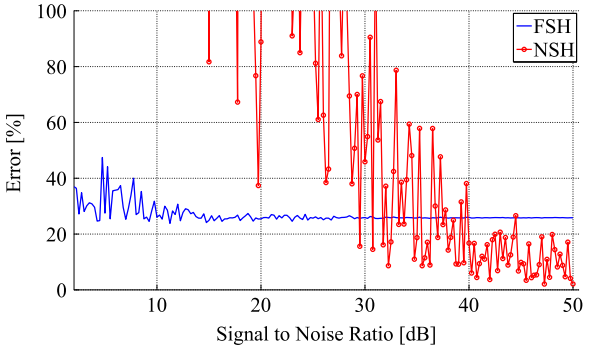

Fig. 11. Quadratic errors as functions of Signal to Noise Ratio (SNR) for the frequency band [10:3500] Hz for FSH (solid line) and NSH (circle).

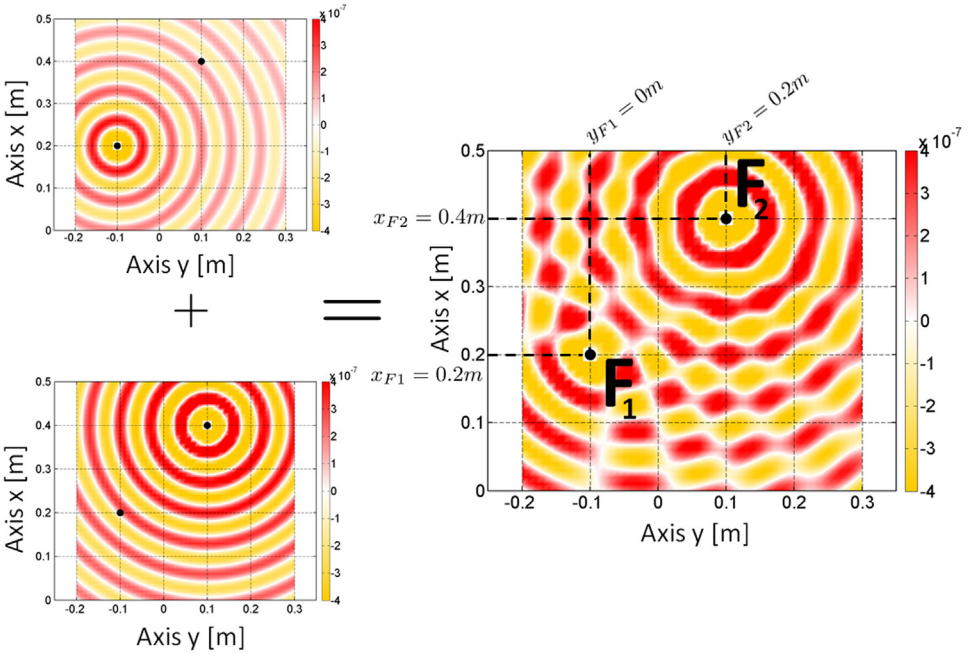

Fig. 12. Displacement field $\overline{w}_{\mathrm{sum}}(x, y)$ of an infinite plate excited by 2 harmonic forces F_1 and F_2 (real part). On the right hand side is the sum of the contribution $\overline{w}_{F1}(x, y)$ (on the top left hand side) and $\overline{w}_{F2}(x, y)$ (on the bottom left hand side) produced respectively by forces F1 and F2.

case for NSH.

5. Numerical experiment on an infinite plate

The purpose of this section is to show how to find the displacement field due to a specific force when two forces are applied to a plate. The aim is then to separate the displacements generated by two harmonic point forces applied to an infinite plate. As in Section 4.3, Eq. (12) is used to simulate the displacement field with the same physical parameters ($E=69\times 10^9$ Pa, $\rho=2700$ kg/m^3, $\nu=0.346$) at frequency 2000 Hz. The force $F_1=0.5$ N generates the $\overline{w}_{F1}$(x,y) displacement field and $F_2=2\times F_1=1$ N produces the displacement field $\overline{w}_{F2}(x,y)$. The total simulated displacement is $\overline{w}_{\text{sum}}(x,y)=\overline{w}_{F1}(x,y)+\overline{w}_{F2}(x,y)$ and is illustrated in Fig. 12. The point forces F_1 and F_2 are respectively located at the co-ordinates $(-0.1,0.2)$m and (0.1,0.4) m in x and y directions. The holograms needed in FSH are respectively located at the positions, $y_{h1}=0$ and $y_{h2}=0.01$ m. The holograms are defined by N=401 points in the x direction separated by $\Delta_x=0.01$ m. The length of the holograms is $L_x=4$ m.

The principle of vibratory field separation is applied to identify the contributions (that is to say the displacement fields) of each point force by measuring the displacement due to both forces on the holograms. Holograms are positioned in the far-field and the coefficients are determined solving the system of Eq. (10). The reference displacement field $\overline{w}_{\text{sum}}(x,y)$ is plotted in Fig. 12. By only using $C^{\text{F}}_{\text{mix}}$ and $C^{\text{B}}_{\text{mix}}$ (Eq. (9)) in the vibratory field separation process, Structural Holography isolates the waves coming from the left side of holograms (with $C^{\text{F}}_{\text{mix}}$) to those coming from the right (with $C^{\text{B}}_{\text{mix}}$). The fields $\overline{w}^{\text{rec}}_{F1}$ and $\overline{w}^{\text{rec}}_{F2}$ reconstructed by FSH (Fig. 13) are very similar to the reference ones (Fig. 12). The initial limitation of Structural Holography theory is clearly visible here: the reconstruction area is restricted to zones with no external forces. In the present case, these zones are defined:

- between -0.1 m and $+\infty$ for field $\overline{w}^{\text{rec}}_{F1}$,
- between $-\infty$ and $+0.1$ m for field $\overline{w}^{\text{rec}}_{F2}$,
- between -0.1 m and $+0.1$ m for field $\overline{w}^{\text{rec}}_{\text{sum}}$

This point can be clearly seen as a limitation of applications of Structural Holography when comparing to classical force reconstruction methods like FAT [9,10] or the source separation technique [23]. However, one has to keep in mind that Structural Holography does not need the measurement of the whole field like the cited methods. As a consequence, the field of applications of Structural Holography is evidently different than the one of classical methods. This will be addressed more precisely in the following sections.

To better evaluate the performances of FSH, the reconstructed displacement $\overline{w}^{\text{rec}}_{F1}(x,y)$ is presented as a function of x (Fig. 14) and y (Fig. 15) axes and compared to the reference displacement $\overline{w}_{F1}(x,y)$. Although $F_1=F_2/2$, one observes a good estimation of the separated displacements compared to the reference for either propagation or back-propagation of field produced by point force F_1. The comparison of the real parts of the displacement obtained by the reference calculation and by FSH as a function of y is presented in Fig. 15. The displacement amplitude near the force is different (error of 31% at $d_{F1}=1$ cm where d_{F1} is the distance between the reconstructed point displacement and the force F_1). As shown in Section 4,

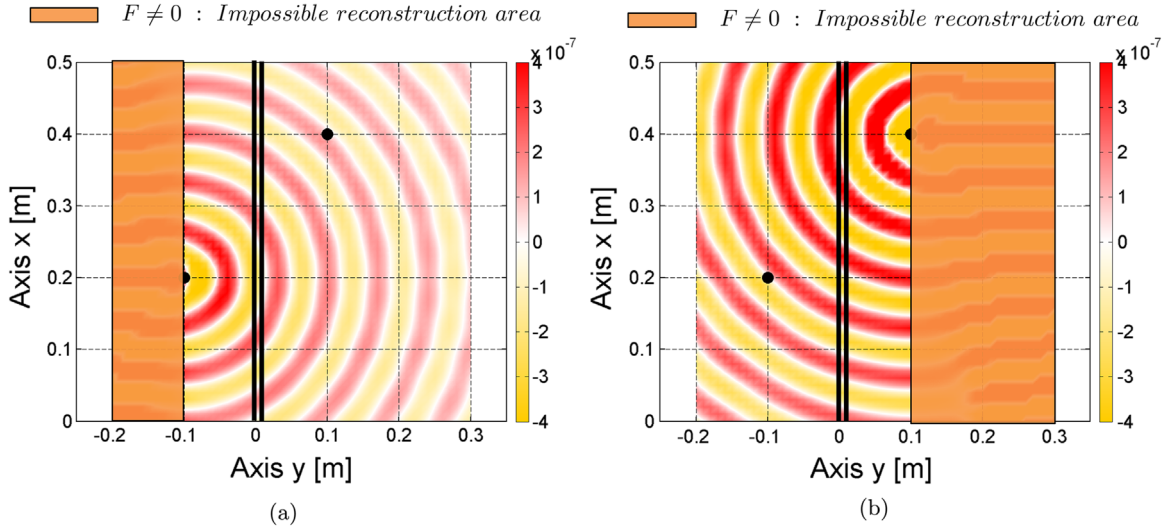

Fig. 13. Reconstructed displacement $w^{\text{rec}}_{F1}(x,y)$ (a) and reconstructed displacement $w^{\text{rec}}_{F2}(x,y)$ (b) computed with Eq. (9). The two vertical lines show the hologram positions.

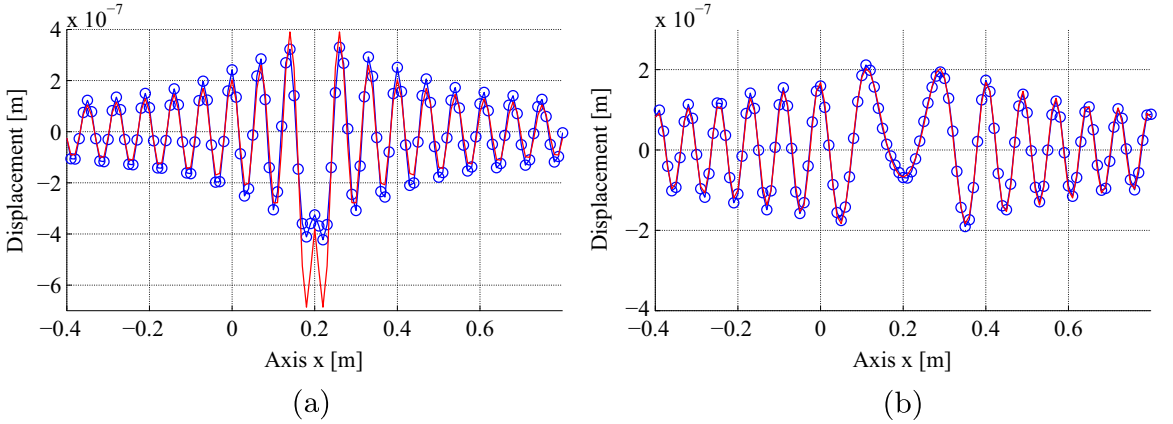

Fig. 14. Reconstructed displacement for the position (a) $y=-9$ cm (back-propagation) and (b) $y=8$ cm (propagation) computed by FSH (circle) compared to reference displacement (in solid line).

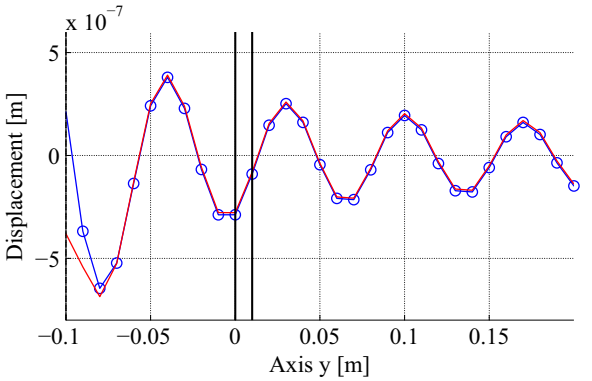

Fig. 15. Reconstructed displacement at $x=21$ cm computed by FSH (circle) compared to reference displacement (in solid line). $y=0$ cm is the hologram position y_{h1} (vertical solid lines).

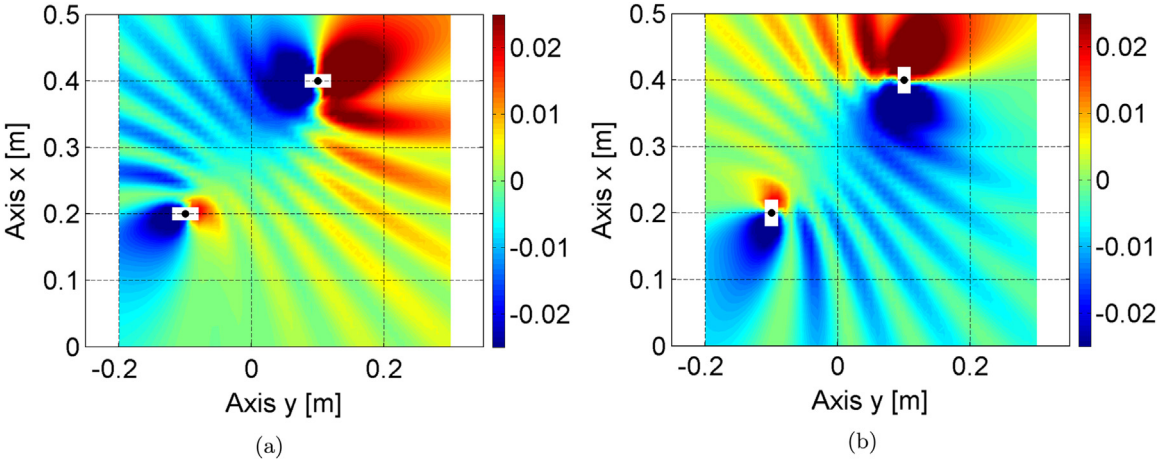

Fig. 16. Structural intensity I_x as a function of x (a) and I_y as a function of y (b) obtained from the reference displacement $\overline{w}_{\mathrm{sum}}(x, y)$.

the FSH formulation does not take into account the complete evanescent behavior and necessitates only two holograms. Moreover, the filter operation limits the information present in the high wave number of coefficient C^{F}_{mix}. This loss of information causes this difference of amplitude. However, this difference is localized near the force (the reconstruction errors is less than 6 % at $d_{F1}=2$ cm). Therefore, Structural Holography allows to separate the displacements fields of sources and to reconstruct them with a good accuracy.

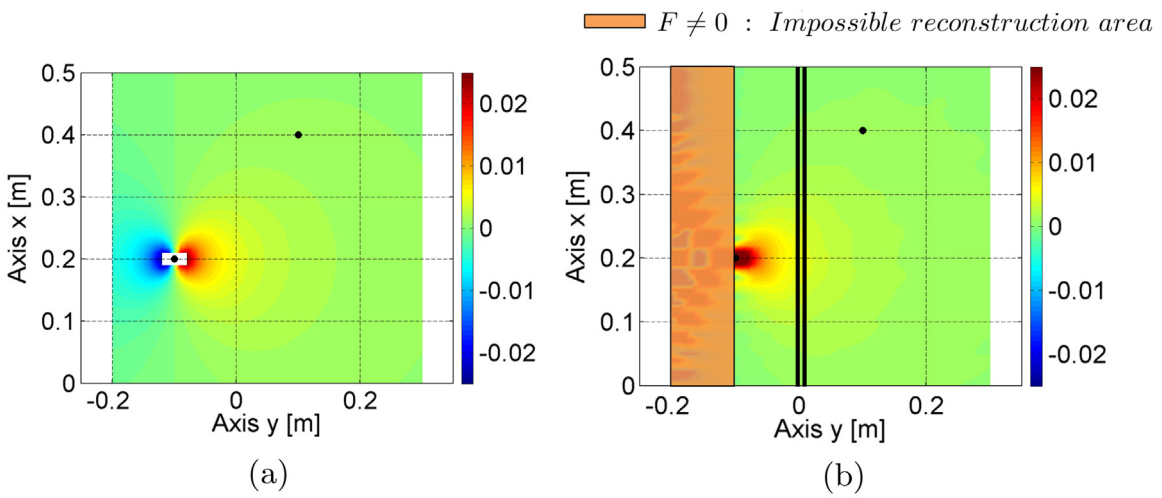

Fig. 17. Structural intensity I_x obtained (a) from reference displacement $\overline{w}_{ref}$ and (b) from the reconstructed displacement. The two vertical lines represent the hologram positions (2 holograms lines).

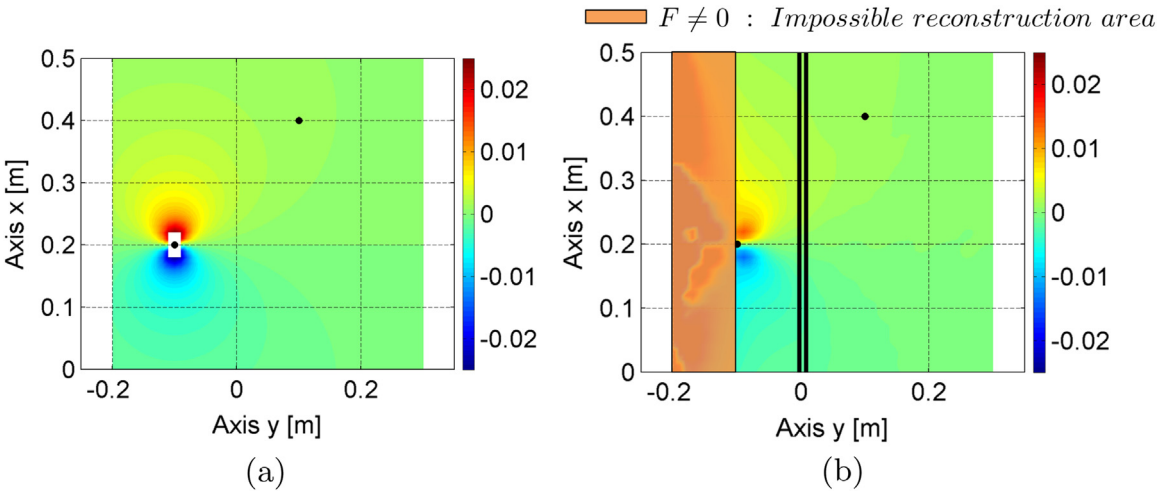

Fig. 18. Structural intensity I_y obtained (a) from reference displacement $\overline{w}_{ref}$ and (b) from the reconstructed displacement. The two vertical lines represent the hologram positions (2 holograms lines).

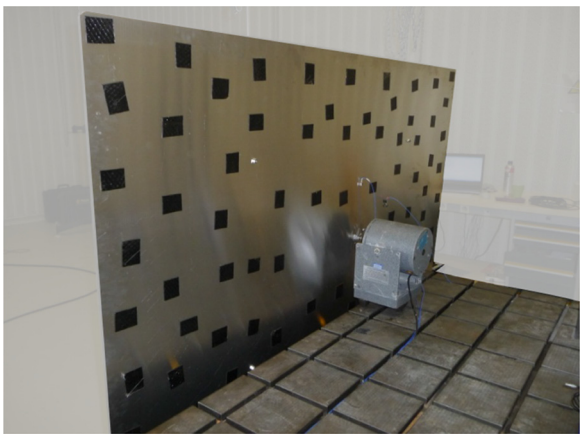

Fig. 19. Experimental setup. An aluminium plate is excited by a dynamics shaker.

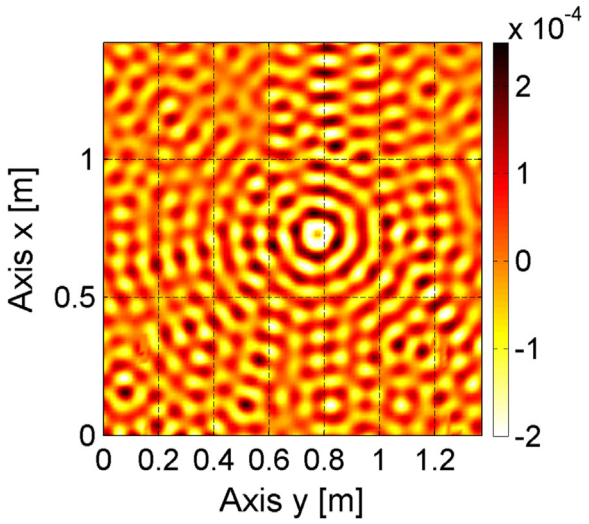

Fig. 20. Directly measured displacement field of an aluminium plate excited by a shaker with a pseudo random signal at frequency $f = 1418$ Hz.

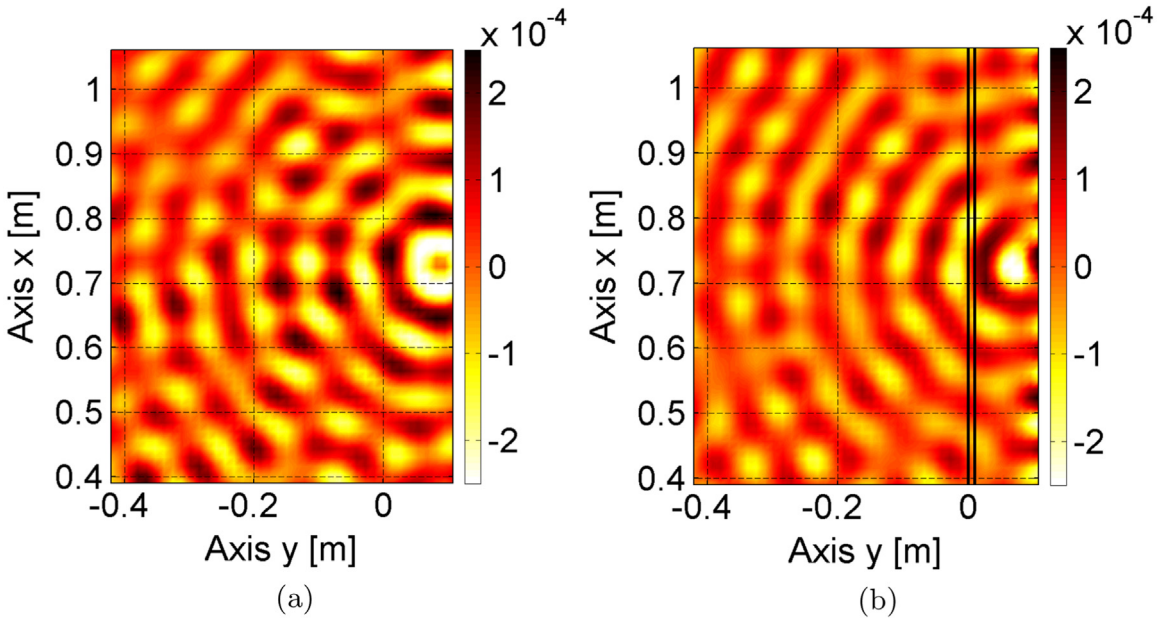

Fig. 21. (a) Reference displacement and (b) reconstructed displacement by structural holography. The two vertical lines represent the hologram positions.

6. Structural intensity

As already shown, Structural Holography allows to reconstruct the displacement field due to a force despite the presence of other forces acting on the plate. It is the separation vibratory field principle. However, the knowledge of the displacement or velocity field does not provide sufficient information to localize the forces applied on the plate. Thereby, a post processing which consists in computing the structural intensity using the reconstructed displacement is proposed in the present section. The interest in computing the structural intensity arises for practical reasons: net energy flow distribution gives information of energy transmission paths and positions of sources and sinks of mechanical energy [7].

The Structural Intensity of the flexural waves in a plate (or density of the energy flow per length unit [W/m]), is a vector quantity which can be expressed from the velocity field [2]. The formulation used here is a simplified formula of the Structural Intensity presented by Pascal [30,31] in far-field and free field conditions:

$$I \approx \sqrt{DM_s}\ \mathrm{Im}\{v\nabla v^*\}, \tag{16}$$

where Im denotes the imaginary part, M_s the mass per unit of area, $D = \dfrac{Eh^3(1+j\eta)}{12(1-\nu^2)}$ and v is the velocity field. This

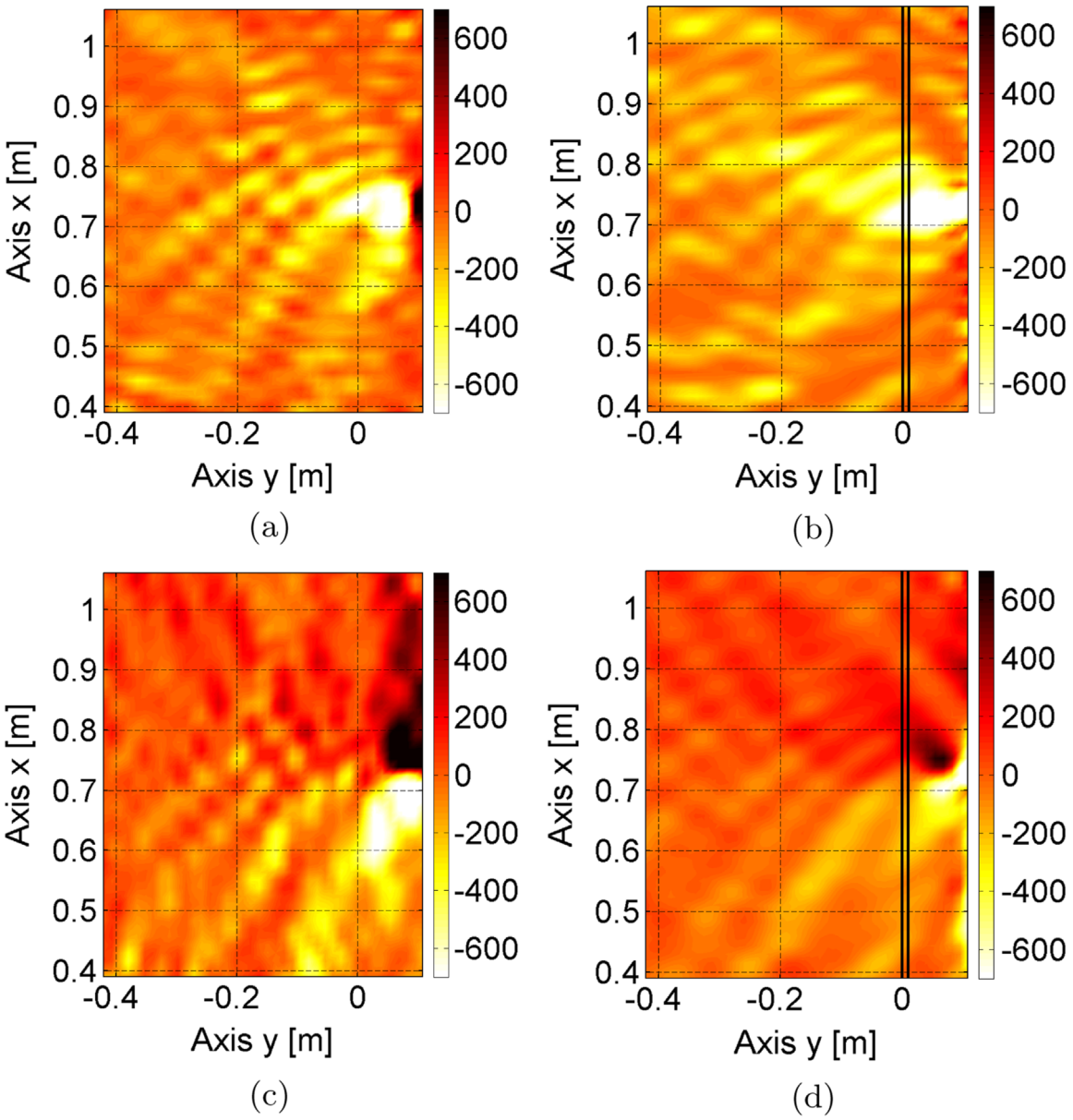

Fig. 22. Structural intensity in x and y directions at frequency 1418 Hz. (a) I_x and (c) I_y obtained from reference displacement field. (b) I_x^{rec} and (d) I_y^{rec} obtained from displacement field reconstructed with FSH. The two vertical lines represent the hologram positions.

formulation describes with good accuracy the flow outside the vortex area and gives an exact quantitative evaluation of the total flow when the measures are realized in the far-field [31].

Moreover the intensity represented by Eq. (16) is dominated by the irrotational part of the intensity field that is very useful to localize energy sources and sinks. The rotational part indicates how the energy loops, while the irrotational intensity indicates how the energy flows from the source towards the far-field. Therefore, for an hologram position in the far-field, the irrotational intensity gives a better representation of structural energy because the masking effects of energy loops that are related to the rotational intensity is not considered [32].

The structural intensity of the reference displacement $\overline{w}_{sum}$ is computed with Eq. (16). The structural intensity fields Ix and Iy are shown in Fig. 16(a) and (b), respectively. As can be seen, the influence of force F_1 is somewhat masked by the one of force F_2 because the amplitude of F_2 is two times higher than the amplitude of F_1.

The structural intensity fields I_x and I_y, computed on the reference displacement $\overline{w}_{F1}$(x,y) generated by force F_1 only, are plotted in Fig. 17(a) and Fig. 18(a) respectively. They are compared to the structural intensity I_{x1}^{rec} and I_{y1}^{rec}, computed on the reconstructed displacement $\overline{w}_{F1}^{rec}(x, y)$ obtained by FSH after applying the separation principle to isolate the effect of force F_1. In the valid reconstruction zone, the reference and the reconstructed intensity fields agree very well and the position of

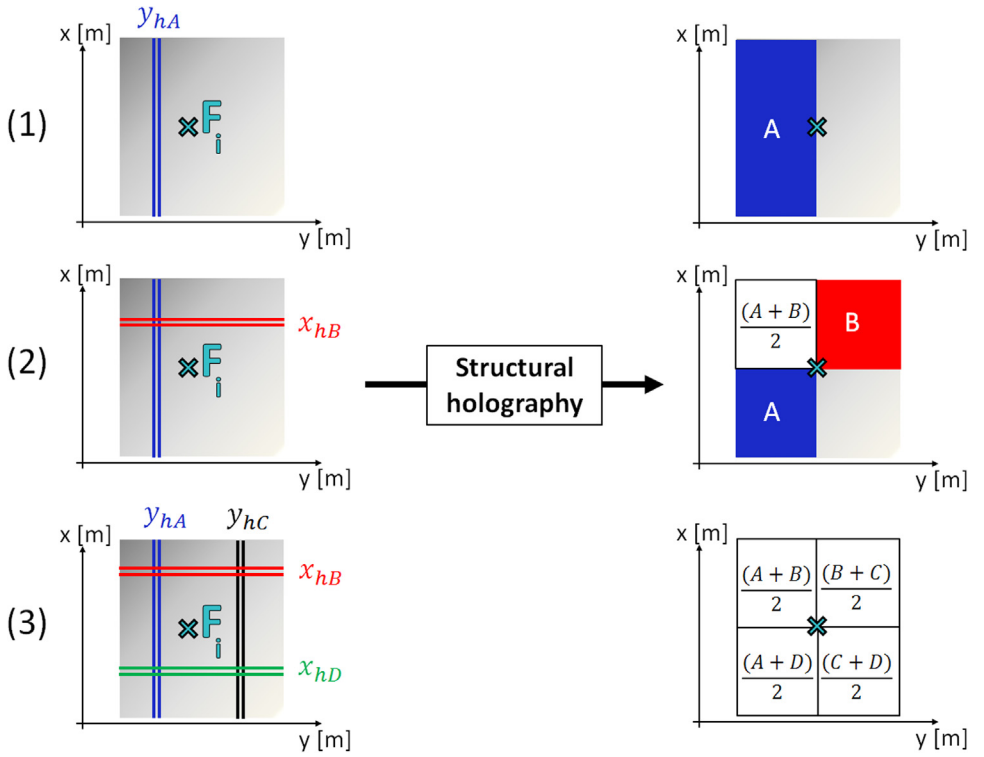

Fig. 23. Synopsys of Structural Holography to identify the force behavior on the entire force application area.

force F_1 is clearly visible using this intensity post processing on FSH results.

The structural intensity I_{x1}^{rec}, allows a good localization of the force F_1 and a good amplitude estimation (Fig. 17). The intensity I_{y1}^{rec} computed on dimension y (Fig. 18) does not yield results equal to the reference I_{y1} (Fig. 18(a)). Indeed, at coordinates (0,21;- 0.08), the error on the intensity amplitude is 15% whereas at the same position the error for I_{x1}^{rec} is about 2,5%. The hologram is on x axis and does not allow the measure of all the phenomena on dimension y. This hologram configuration causes a slight underestimation of I_{y1}^{rec}.

One of the most important features of the structural intensity is its ability to localize and characterize the sources of energy on a plate [33]. In the present work, the use of structural intensity on the reconstructed displacement shows good localization and identification of the intensity field caused by the force F_1. Therefore, additional useful information is provided by this post-processing easily applicable to Structural Holography.

7. Experimental results

This section illustrates the application of the method in real conditions. Measurements are made on a rectangular aluminum plate ($E=69\times\ 10^9$ Pa, $\rho=2700$ kg/m^3, $\nu=0{,}346$), hanged from one side. The dimensions of the plate are 212×144 cm. The thickness is $h=1$ mm. The plate has an average damping of 1 % mainly due to the presence of small viscoelastic patches glued on the plate. Measurements were performed on a grid of 107 by 101 points with an inter-space of $\Delta_x=\Delta_y=1.35$ cm on a measurement plane of $L_x\times L_y$ where $L_x=144{,}45$ cm and $L_y=137$ cm.

The plate was excited with a MB dynamics MODAL 50 shaker (Fig. 19). The excitation force was a pseudo random signal, applied to the point $x_F=73$ cm and $y_F=77$ cm in the scanned zone. The displacement field on the plate was measured with a Polytec PSV-400 laser vibrometer positioned at 6 m from the plate. 20 averages were applied for each mesh point. As an example, the measured displacement at frequency $f=1418$ Hz is illustrated in Fig. 20. It can be taken as the reference in the following.

The hologram positions are $y_{h1}=63$ cm and $y_{h2}=63+1.35$ cm. Thereafter, the reference and reconstructed displacement fields are illustrated relatively to the hologram positions. The holograms are defined by $N_x=107$ points in x direction separated by Δ_x. The length of the holograms is L_x. In these real experiments, $k_x^{max}=232$, 7 rad/m and $\Delta_{kx}=4{,}35$ rad/m.

Due to the plate size and the damping, the displacement field is mainly a direct field and so is rather not reverberant. This is why force position is clearly visible on reference measurement in Fig. 20. In that case, forth and back waves identified by Structural Holography will mainly be due to waves generated by the force. This test case has been chosen as a validation test for Structural Holography. As the holograms are positioned in the far-field, FSH is used to compute the plate displacement.

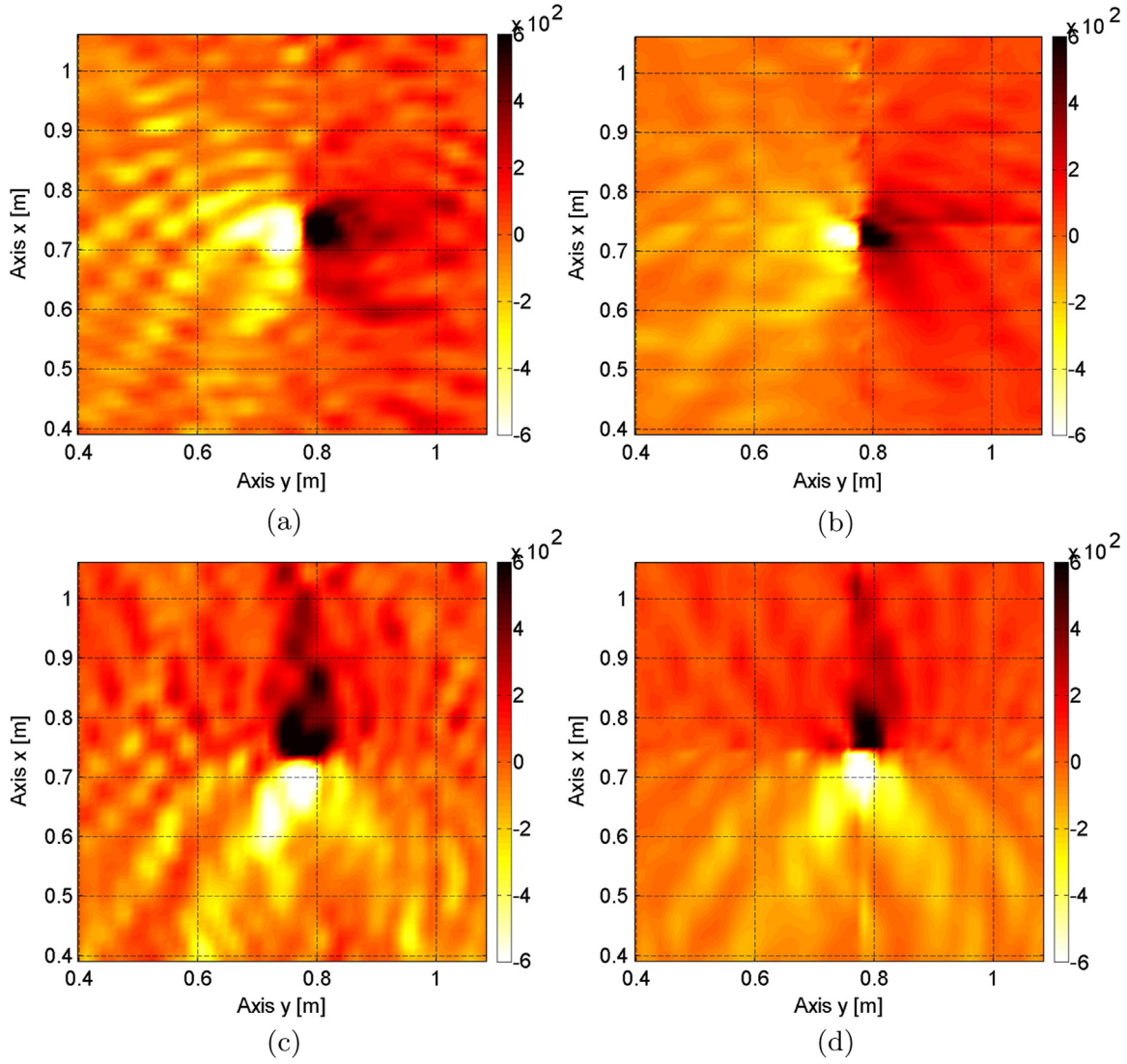

Fig. 24. Structural intensity in x and y directions at frequency 1418 Hz. (a) I_x and (c) I_y obtained from reference displacement field. (b) I_x^{rec} and (d) I_y^{rec} obtained from displacement field reconstructed with FSH.

Result is illustrated in Fig. 21 and compared with the reference displacement. The comparison between reference and FSH result is satisfactory. Both maps show fields with same wavelength, centred on the same point.

Structural intensity I_x and I_y are computed using the reference and the reconstructed displacement field and plotted in Fig. 22. In this real experiment, the identification of intensity fields using FSH gives good results compared to direct measurements. The intensity field I_x is well reconstructed in both spatial distribution and amplitude using only measures on two holograms. In y direction, the reconstruction is not as good mainly because of the holograms direction (x axis).

To reconstruct the entire force behavior, Structural Holography is applied in this Section from few hologram positions on x and y dimensions. The process is schematized in Fig. 23. The holograms y_{hA} allow to reconstruct the displacement on A area (step 1). The holograms x_{hB} compute the displacement on B area and the common area between the reconstructed displacements A and B is computed with (A+B)/2 (step 2). Step 3 is the result of step 2 reproduced all around the force F_i. By following this process, the entire displacement is computed. The structural intensity I_x and I_y are identified and illustrated in Fig. 24. The filter applied on the coefficients and the average between the reconstructed displacements described by step 2 decrease the measurement noise. As shown in Section 6, the estimation of intensity field in direction of the holograms lines (I_y in Fig. 18(b)) is slightly underestimated compared to reference. This underestimation is not visible in Fig. 24 thank to the averaging of results obtained with holograms with different orientation. Therefore, by using this process, Structural Holography identifies the whole intensity field present around the force with only few holograms.

8. Conclusion

A new approach based on the same principle as Near-field Acoustic Holography was proposed to reconstruct the displacement field of a plate with a limited number of measurements. This method called Structural Holography is based on the back-propagation process performed in the k-space domain by using the Spatial Fourier Transform on lines. Unlike the classical methods, Structural Holography is not dedicated to estimation of force distribution by measuring displacement on the whole surface of the structure but permits to reconstruct displacement fields with only 2 or 4 measurements lines (holograms). Moreover, as Structural Holography expression can be separated in two kinds of waves, the forth waves and backwaves, this method is thus a vibratory field separation method.

In the theoretical background, the general formulation of Structural Holography presents 4 coefficients. 2 coefficients characterize purely evanescent waves. As the evanescent waves decrease quickly with the distance to force or boundary conditions, the amplitudes of these can be almost null at the positions of holograms and induce error in the back propagation process. Therefore, two versions of Structural Holography are presented in this paper: the Near-field Structural Holography (NSH) process composed 4 holograms and the Far-field Structural Holography (FSH) process, where the evanescent waves are neglected (2 holograms). In practice, FSH is more useful than NSH because it gives satisfactory results for many configurations. FSH provides an accurate reconstruction with holograms positioned in the far-field and in the near-field. Moreover, results are reliable whatever the Signal-to-Noise Ratio.

The vibratory field separation by Structural Holography is applied to a numerical experiment with an infinite plate. Two forces with different amplitudes are separated and the displacement of the two forces is reconstructed by FSH. A post processing, which consists in computing the structural intensity on the reconstructed displacement by FSH, is applied and gives additional useful information on the force behavior.

Finally, Structural Holography is experimentally applied to localize and identify the vibratory field produced by a source. It is generated by a shaker in the case of an experimental measure. The force is firstly identified with two holograms positioned on one dimension and the operation is repeated around the force application area to compute the entire intensity field. To conclude, Structural Holography allows to localize and identify the vibratory field around a force without knowledge of its position with only few holograms positioned in the far-field.

Acknowledgments

This work was supported by the Labex CeLyA of Université de Lyon, operated by the French National Research Agency (ANR-10-LABX-0060/ANR-11-IDEX-0007).

This work has been made possible because of the financial support of the French Fond Unique Interministériel 15" (FUI, Interministerial Funds) in the framework of the TESSA project.

References

[1] E.G. Williams, J.D. Maynard, E. Skudrzyk, Sound source reconstructions using a microphone array, *J. Acoust. Soc. Am.* 68 (1) (1980) 340–344.
[2] G. Pavić, Measurement of structure 530 borne wave intensity, Part I: formulation of the methods, *J. Sound Vib.* 49 (2) (1976) 221–230.
[3] D. Noiseux, Measurement of power flow in uniform beams and plates, *J. Acoust. Soc. Am.* 47 (1) (1969) 238–247.
[4] Y. Zhang, J.A. Mann III, Measuring the structural intensity and force 535 distribution in plates, *J. Acoust. Soc. Am.* 99 (1) (1996) 345–353.
[5] Y. Zhang, J.A. Mann III, Examples of using structural intensity and the force distribution to study vibrating plates, *J. Acoust. Soc. Am.* 99 (1) (1996) 354–361.
[6] L. Gavrić, Influence de modifications locales sur le flux d'énergie dans les structures à paroi mince (Influence of local modifications on energy flow in thin-walled structures), (Ph.D. thesis), Université de Technologie de Compiègne, 1991.
[7] L. Gavrić, G. Pavić, A finite element method for computation of structural intensity by the normal mode approach, *J. Sound Vib.* 164 (1) (1993) 29–43.
[8] L. Gavrić, U. Carlsson, L. Feng, Measurement of structural intensity using a normal mode approach, *J. Sound Vib.* 206 (1) (1997) 87–101.
[9] C. Pézerat, Méthode d'identification des efforts appliqués sur une structure vibrante, par résolution et régularisation du problème inverse (Identification of Forces Applied on Vibrating Structures by Resolution and Regularization of the Inverse Problem), (Ph.D. thesis), Institut National des Sciences Appliquées de Lyon, 1996.
[10] C. Pézerat, J.-L. Guyader, Force analysis technique: reconstruction of force distribution on plates, *Acta Acust. United Acust.* 86 (2) (2000) 322–332.
[11] C. Pézerat, J.-L. Guyader, Two inverse methods for localization of external sources exciting a beam, *Acta Acust.* (1995) 1–10.
[12] M. Djamaa, N. Ouelaa, C. Pézerat, J.-L. Guyader, Mechanical force identification of a finite cylindrical shell by an inverse method, *Acta Acust. United Acust.* 92 (2006) 398–405.
[13] M. Djamaa, N. Ouelaa, C. Pézerat, J.-L. Guyader, Reconstruction of a distributed force applied on a thin cylindrical shell by an inverse method and spatial filtering, *J. Sound Vib.* 301 (3-5) (2007) 560–575.
[14] C. Pézerat, Q. Leclère, N. Totaro, M. Pachebat, Identification of vibration excitations from acoustic measurements using near field acoustic holography and the force analysis technique, *J. Sound Vib.* 326 (3-5) (2009) 540–556.
[15] A. Berry, O. Robin, Identification of spatially correlated excitations on a bending plate using the Virtual Fields Method, *J. Sound Vib.* 375 (2016) 76–91.
[16] A. Berry, O. Robin, F. Pierron, Identification of dynamic loading on a bending plate using the Virtual Fields Method, *J. Sound Vib.* 333 (26) (2014) 7151–7164.
[17] J. D. Maynard, E.G. Williams, Y. Lee, Nearfield acoustic holography (NAH): I - Theory of generalized holography and the development of NAH, The Journal of the Acoustical Society of America, vol. 78 (4).
[18] W. Veronesi, J.D. Maynard, NearField acoustic holography (NAH) II - Holographic reconstruction algorithms and computer implementation, The Journal of the Acoustical Society of America, vol. 81 (5).
[19] D. Greussing, M. Cavallari, H.A. Bonhoff, B.A.T. Petersson, The conception of structure-borne-sound-based near-field holography, *J. Sound Vib.* 331 (18) (2012) 4132–4144.

[20] J.-H. Thomas, V. Grulier, S. Paillasseur, J.-C. Pascal, J.C. Le Roux, Real-time near-field acoustic holography for continuously visualizing non-stationary acoustic fields, *J. Acoust. Soc. Am.* 128 (6) (2010) 3554–3567.
[21] J. Hald, Time domain acoustical holography and its applications, *J. Sound Vib.* 35 (2) (2001) 16–25.
[22] E.G. Williams, Regularization methods for near-field acoustical holography, *J. Acoust. Soc. Am.* 110 (4) (2001) 1976–1988.
[23] M.-T. Cheng, J.A. Mann III, A. Pate, Wave-number domain separation of the incident and scattered sound field in Cartesian and cylindrical coordinates, *J. Acoust. Soc. Am.* 97 (4) (1995) 293–303.
[24] A.W. Leissa, Vibration of plates, Tech. rep., DTIC Document, 1969.
[25] M. Lee, J.S. Bolton, L. Mongeau, Application of cylindrical near-field acoustical holography to the visualization of aeroacoustic sources, *J. Acoust. Soc. Am.* 114 (2) (2003) 842–858.
[26] J. Tukey, *An Introduction to the Calculations of Numerical Spectrum Analysis*, B.Harris, 1967.
[27] K. Saijyou, Measurement of structural intensity using boundary element method-based nearfield acoustical holography, *J. Acoust. Soc. Am.* 121 (6) (2007) 3493–3500.
[28] J.-C. Pascal, T. Loyau, J.A. Mann III, Structural intensity from spatial Fourier transformation and BAHIM acoustical holography method, International Congress on intensiy techniques, 1990.
[29] E.G. Williams, Fourier Acoustics Sound Radiation and Nearfield Acoustical Holography, academic press, London Edition, 1999.
[30] J.R.F. Arruda, P. Mas, Localizing energy sources and sinks in plates using power flow maps computed from laser vibrometer measurements, *Shock Vib.* 5 (4) (1998) 235–253.
[31] J.-C. Pascal, T. Loyau, X. Carniel, Complete determination of structural intensity in plates using laser vibrometers, *J. Sound Vib.* 161 (3) (1993) 527–531.
[32] N.B. Roozen, J.L. Guyader, C. Glorieux, Measurement-based determination of the irrotational part of the structural intensity by means of test functional series expansion, *J. Sound Vib.* 356 (2015) 168–180.
[33] E.G. Williams, H. Dardy, R.G. Fink, A technique for measurement of structure-borne intensity in plates, *J. Acoust. Soc. Am.* 78 (6) (1985) 2061–2068.